Polym. Bull. (2011) 67:1945–1959
DOI 10.1007/s00289-011-0613-x

ORIGINAL PAPER

Non-isothermal crystallization of monomer casting polyamide 6/functionalized MWNTs nanocomposites

Shangchang Qiu · Yuying Zheng · Anran Zeng · Yong Guo · Baoming Li

Received: 7 December 2010 / Revised: 14 May 2011 / Accepted: 20 August 2011 /
Published online: 28 August 2011

Abstract Monomer casting polyamide 6(MCPA6)/toluene 2,4-diisocyanate functionalized multi-walled carbon nanotubes (MWNTs-NCO) nanocomposites were prepared via in situ anionic ring opening polymerization, and the non-isothermal crystallization behavior of the nanocomposites were investigated by differential scanning calorimetry with various cooling rates. The commonly used Avrami, Ozawa, Mo, and Urbanovici–Segal models were employed to analyze the non-isothermal crystallization data and the validity of the models on the process of MCPA6 and its nanocomposites was discussed, where Mo and Urbanovici–Segal models could well describe the non-isothermal crystallization process for the samples. The results revealed that MWNTs could accelerate the crystallization process of MCPA6, attributing to the nucleating effect of the nanofillers. Finally, the effective energy barrier for non-isothermal crystallization was evaluated as a function of the relative crystallinity by applying an isoconversional method.

Keywords Monomer casting polyamide 6 · Carbon nanotubes · Non-isothermal crystallization · Crystallization kinetics

Introduction

Polyamide 6 (PA6), also known as nylon 6, is one of the prominent members of the polyamides. It combines excellent properties and competitive price, making it the most used type of polyamide worldwide [1]. PA6 could be synthesized via either anionic polymerization or hydrolytic reaction. Prepared via in situ anionic ring

S. Qiu · Y. Zheng (✉) · A. Zeng · Y. Guo
College of Chemistry and Chemical Engineering, Fuzhou University, Fuzhou 350108, Fujian, China
e-mail: yyzheng_217@yahoo.cn

Y. Zheng · B. Li
College of Materials Science and Engineering, Fuzhou University, Fuzhou 350108, Fujian, China

opening polymerization, monomer casting PA6 (MCPA6) has many advantages over normal PA6 prepared by hydrolytic polymerization due to its high molar mass and high degree of crystallinity [2, 3]. Recently, organic/inorganic particles-filled nanocomposites based on polymer matrix have attracted much interest since they exhibit greatly improved mechanical, rheological properties [4, 5], and some unexpected hybrid properties [6]. Among the different nanoparticles used in polymer composites, Carbon nanotubes (CNTs), which could be classified into two types: single-walled carbon nanotubes (SWNTs) and multi-walled carbon nanotubes (MWNTs), have attracted much attention because of its unique structure, high surface area, great mechanical property, excellent electrical and thermal conductivity, etc. Such properties make CNTs favorable candidates for the reinforcements on polymer's intensity and electrical conductivity [7, 8].

It is well-known that crystallization behaviors play an important role in the physical, chemical, and mechanical properties of polymers. Therefore, it is of great significance to take the crystallization into account for the study of polymer process [9–12]. The research on non-isothermal crystallization is more technically important than on isothermal crystallization since most practical processing techniques proceed under non-isothermal conditions [13]. The crystallization behavior of filler-reinforced polymers has been studied extensively [14–20]. Li et al. [21] have investigated the non-isothermal crystallization kinetics of MWNTs nanocomposites based on normal polycondensation PA 6 matrix. However, as far as we know, no studies about the effects of MWNTs on the non-isothermal crystallization kinetics of MCPA6 have been published.

In this study, MCPA6/MWNTs nanocomposites were prepared via in situ anionic ring opening polymerization, where MWNTs was functionalized by toluene 2,4-diisocyanate (TDI) through esterification. The non-isothermal crystallization kinetics was analyzed using theoretical models, namely Avrami, Ozawa, Mo, and Urbanovici–Segal model. The effective energy barrier of non-isothermal crystallization was calculated as a function of the relative crystallinity by an isoconversional approach.

Experimental

Materials

ε-caprolactam (CL), ethyl acetate, and sodium hydroxide (NaOH) used in this study were purchased from Sinopharm Chemical Reagent Co., Ltd., China. Commercial hydroxyl functionalized multi-walled carbon nanotubes (MWNTs-OH with 2.97 wt% OH) were obtained from Shenzhen Nanotech Port Co., Ltd., China. TDI was made by Mitsui Chemicals Inc., Japan.

Commercial MWNTs-OH functionalization

About 0.25 g of MWNT-OH and 0.5 mL of TDI was dispersed in 50 mL of ethyl acetate under vigorous stirring, and the reaction was undertaken at 80 °C for 4 h.

Subsequently, the obtained products were filtrated and extracted with ethyl acetate at 90 °C for 24 h to completely remove the unreacted TDI. After being dried, multi-walled carbon nanotubes (MWNTs-NCO) was obtained.

Nanocomposites preparation

0.3 wt% of MWNTs-NCO was dispersed in the melted CL under vacuum for 0.5 h to remove the moisture. Then NaOH was added into the system at 140 °C for another 0.5 h, and as the activator TDI was dropped, the final mixture was immediately poured into a preheated reactor in a heavily insulated oven at 160 °C and polymerized for 30 min. Finally, the PA6/MWNTs nanocomposites were obtained after the extraction of the polymer with boiling water. For the polymerization, the concentration of initiator was kept constant at 0.2 wt% and the amount of activator was kept constant at 0.3 wt%.

Characterization

Fourier transform infrared (FT-IR)

FT-IR spectra of MWNTs-OH and MWNTs-NCO (KBr pellet) was recorded on a Perkin-Elmer Lambda 900 FT-IR spectrometer with the wave number 4,000–400 cm^{-1}.

Monomer conversion

To determine the monomer conversion, the sample (about 5–10 g, m_0) were extracted with Soxhlet apparatus for 24 h, using water as the extracting medium for the removal of the monomer and oligomers. After the extraction, the sample was dried under vacuum at 80 °C till it showed no weight variation (m_1). The monomer conversion M_{con} was calculated according to:

$$M_{con} = \frac{m_1 - m_0 X}{m_0(1 - X)} \times 100\% \quad (1)$$

where X was the content of carbon nanotubes (wt%).

Scanning electron microscopy (SEM) observation

The morphology of the fractured surfaces of samples was monitored using a FEI Nova NanoSEM 230 microscope. Samples were kept in liquid nitrogen and then brittle fractured. All considered specimens were gold coated for enhancing conductivity.

Differential scanning calorimetry (DSC) measurement

Differential scanning calorimetry data of both samples were measured on a Perkin-Elmer Diamond DSC to study the non-isothermal crystallization behavior. All DSC

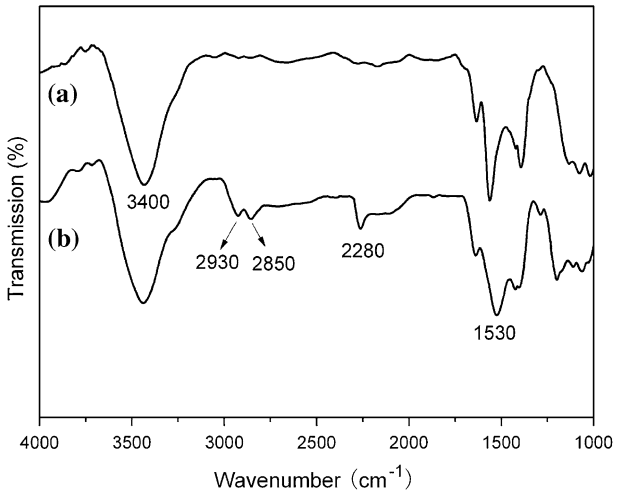

Fig. 1 FT-IR spectra of (*a*) MWNTs-OH and (*b*) MWNTs-NCO

measurements were conducted under nitrogen atmosphere. 10 ± 0.01 mg of the samples were quickly heated to 250 °C and maintained for 5 min to eliminate the thermal history, and then were cooled down to room temperature at a constant cooling rate of 5, 10, 20, and 30 °C min^{-1}, respectively.

Results and discussion

FT-IR characterization

Figure 1 displayed the FT-IR spectra of MWNTs-OH and MWNTs-NCO to investigate the grafting reaction of TDI onto MWNTs-OH. For MWNTs-OH, the peaks at around 3,400 cm^{-1} was attributed to O–H stretching of hydroxyl group. There was an additional peak at 2,280 cm^{-1} for MWNTs-NCO due to the asymmetric stretching of isocyanate group, and the peak at 1,530 cm^{-1} for MWNTs-NCO, characteristic absorption peak of amide band, was ascribed to the esterification of hydroxyl and isocyanate groups. Furthermore, the peaks at 2,930 and 2,850 cm^{-1} for MWNTs-NCO were observed, which was corresponded to C–H stretching of methyl groups of TDI. It was indicated that TDI was grafted onto MWNTs-OH.

Polymerization

The monomer conversion for the polymerization in the presence of MWNTs-NCO and of MWNTs-OH was 98.1 and 97.7%, respectively, while that for the polymerization in the absence of MWNTs was 98.6%. The result showed that either MWNTs-NCO or MWNTs-OH did not hinder the polymerization process.

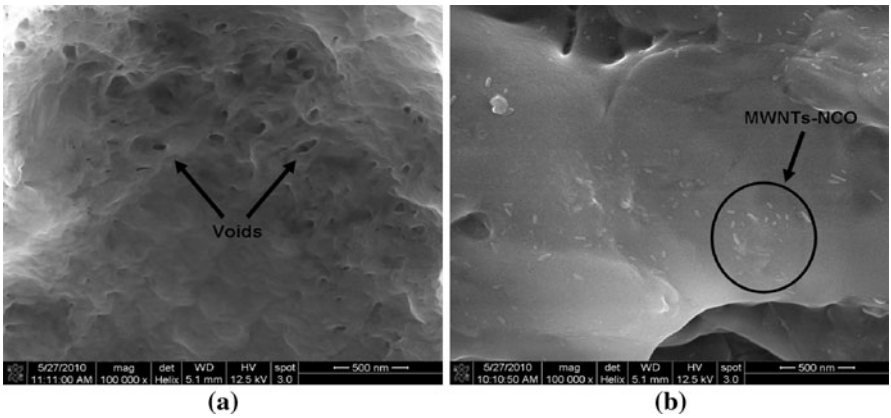

Fig. 2 SEM photography of fractured surface of **a** MCPA6/untreated MWNTs-OH nanocomposites and **b** MCPA6/MWNTs-NCO nanocomposites

SEM characterization

The SEM images showed in Fig. 2 were used to investigate the interfacial bonding between MWNTs and MCPA6. Clearly, the fractured surface of MCPA6 nanocomposites filled with untreated MWNTs shows no MWNTs except some voids, meaning that there is a weak bonding between MCPA6 matrix and MWNTs and thereby MWNTs would be easily pulled out from smooth surfaces. Whereas the functionalized MWNTs was found adhered to the MCPA6 matrix, suggesting that the functionalization of MWNTs with TDI could enhance the interfacial adhesion between MWNTs and MCPA6 matrix. This phenomenon was probably due to that MWNTs-NCO, bearing isocyanate group, could react with CL to form N-carbamated caprolactam moieties from which PA6 chains grew. Moreover, as shown in SEM images, the functionalized MWNTs dispersed more uniformly in PA6 matrix, meaning that the aggregation of carbon nanotubes is reduced with the NCO functionalization.

Non-isothermal crystallization behavior

The analysis on non-isothermal crystallization of polymer via calorimetric methods must be performed with care because of the possible occurrence of thermal gradients within sample and between the furnace and the sample [22]. To avoid thermal gradients, scanning rates should not exceed 1 and 100 °C min^{-1} for samples of 1 g and 1 mg, respectively [23], and the samples should be prepared to be as thin as possible.

The crystallization exotherms of MCPA6 and MCPA6/MWNTs-NCO nanocomposites at various cooling rates are presented in Fig. 3. From these curves, some useful parameters, such as the peak temperature (T_p) and relative crystallinity (X_t) as a function of crystallization temperature can be obtained for describing the non-isothermal crystallization behavior of the system. It was found that as expected, T_p

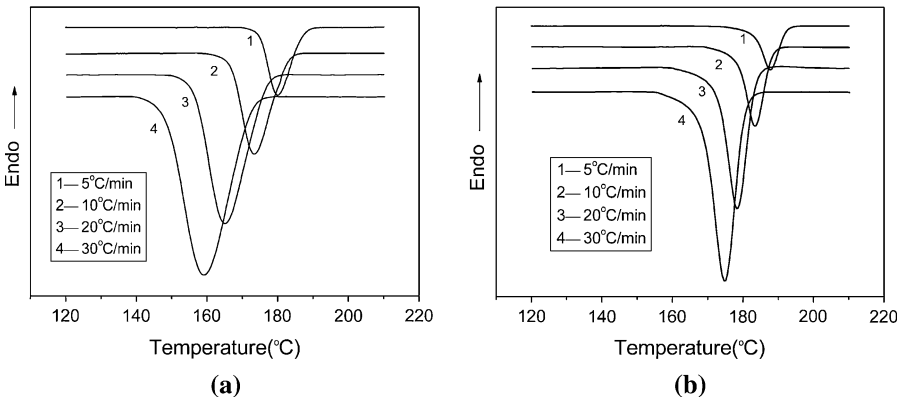

Fig. 3 DSC thermograms of **a** pure MCPA6 and **b** MCPA6/MWNTs-NCO nanocomposites

Table 1 Parameters of sample during non-isothermal crystallization process

Sample	β (°C min^{-1})	n	Z_t (min^{-n})	Z (min^{-1})	Z_c	$t_{1/2}$ (min)	T_p (°C)	ΔH (J/g)
MCPA6	5	3.92	0.03	0.41	0.49	2.25	180.06	48.64
	10	3.23	0.42	0.76	0.91	1.20	173.43	47.81
	20	3.52	1.55	1.13	1.02	0.80	165.22	45.68
	30	3.43	4.06	1.50	1.04	0.60	159.01	44.04
MCPA6/MWNTs-NCO	5	4.23	0.06	0.51	0.57	1.76	187.77	46.65
	10	4.12	0.36	0.78	0.99	0.93	183.49	46.46
	20	4.68	8.17	1.57	1.11	0.57	178.29	47.61
	30	4.52	43.38	2.30	1.13	0.39	174.60	47.54

shifted toward lower temperature and the crystallization temperature range became broader with increasing cooling rates for both pure MCPA6 and MCPA6/MWNTs-NCO nanocomposites. While for a given cooling rates, T_p of MCPA6/MWNTs-NCO nanocomposites was higher than that of pure MCPA6 as listed in Table 1, which could be explained by the nucleation effect of MWNTs-NCO on the crystallization of MCPA6 that makes the PA6 macromolecular segments easily attached to the surface of carbon nanotubes, leading to the crystallization of MCPA6 occurred at a higher temperature. The crystallization enthalpies, ΔH, which is proportional to the degree of crystallinity, decreased for MCPA6 with the increase on cooling rate, whereas that for the nanocomposites is more stable. It means that the degree of crystallinity for pure MCPA6 is more susceptible to the cooling rate than that for the nanocomposites.

Non-isothermal crystallization kinetics

In order to further analyze the non-isothermal crystallization process, the crystallization kinetics of MCPA6 and MCPA6/MWNTs-NCO nanocomposites

were compared. The relative crystallinity as a function of crystallization temperature, X_T, was defined as

$$X_T = \frac{\int_{T_0}^{T} (\mathrm{d}H_c/\mathrm{d}T)\mathrm{d}T}{\int_{T_0}^{T_\infty} (\mathrm{d}H_c/\mathrm{d}T)\mathrm{d}T} \tag{2}$$

where T_0 and T_∞ are the onset and end crystallization temperature, respectively, and T as well as the crystallization temperature at time t. The crystallization temperature T can be transformed to time, t, using the following equation:

$$t = \frac{T_0 - T}{\beta} \tag{3}$$

To quantitatively understand the evolution of the non-isothermal crystallization process, some models have been employed to analyze the non-isothermal crystallization of MCPA6 and its nanocomposites.

Avrami model

The analysis of the relative crystallinity as a function of time, X_t, is usually carried out in the context of Avrami equation [24], which can be expressed as

$$X_t = 1 - \exp(-Z_t t^n) \quad \text{or } X_t = 1 - \exp[-(Zt)^n] \tag{4}$$

where n is the Avrami exponent which is the function of the nucleation process and Z_t is the crystallization rate constant involving both nucleation and growth rate parameters. It was obvious that the dimension of Z_t is given in $(\text{time})^{-n}$ and thereby it is not only the function of the temperature but also a function of the Avrami exponent n. Eq. 4 can be written in another form, where $Z_t = Z^n$. As a result, the use of Z independent of n should be more preferable than use of Z_t. By taking double logarithm of both sides, Eq. 4 can be transformed to that

$$\ln[-\ln(1 - X_t)] = \ln Z_t + n \ln t \tag{5}$$

Figure 4 showed the curve of $\ln[-\ln(1 - X_t)]$ against $\ln t$ for MCPA6 and its nanocomposites, and the curve demonstrated good linearity at low degree of crystallinity. The values of n and Z_t can be calculated from the slops and intercepts of the lines, respectively, and Z was calculated from the respective value of n and Z_t. It should be noted that in non-isothermal crystallization, n and Z_t do not have the same physical significance as in the isothermal crystallization because temperature changes constantly under non-isothermal crystallization. Since the rate of non-isothermal crystallinity depends on the cooling rate, Jeziorny [25] suggested that the rate parameter Z_t should be corrected by cooling rate β, and the final form of this parameter is given by

$$\ln Z_c = \frac{\ln Z_t}{\beta} \tag{6}$$

Thus, the crystallization half time, can be calculated from the corrected constant using the equation

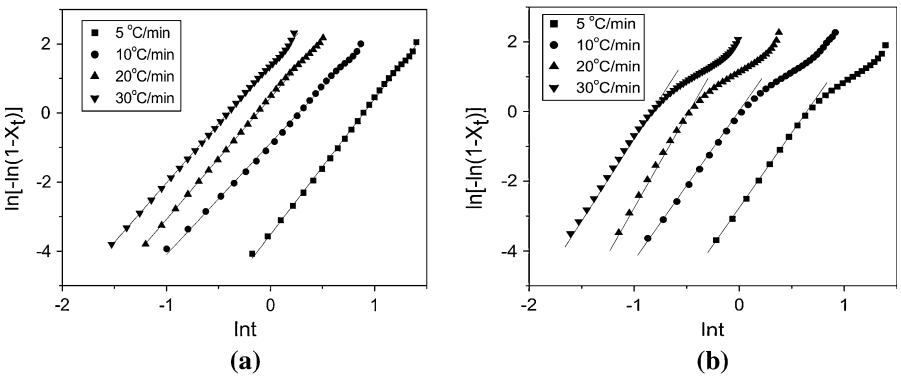

Fig. 4 Plots of $\ln[-\ln(1 - X_t)]$ versus $\ln t$ for non-isothermal crystallization of **a** pure MCPA6 and **b** MCPA6/MWNTs-NCO nanocomposites

$$t_{1/2} = \left(\frac{\ln 2}{Z_c}\right)^{1/n} \tag{7}$$

The results obtained from the Avrami plots and Jeziorny method were listed in Table 1. Exponents n for pure MCPA6 (varied from 3.23 to 3.90) were lower than that for MCPA6/MWNTs-NCO nanocomposites (varied from 4.12 to 4.68), indicating that a change in the nucleation mechanism and/or in the morphology of the spherulites [22] by the effect of MWNTs-NCO. The value of $t_{1/2}$, as expected, decreased with the increase in the cooling rate for both pure MCPA6 and MCPA6/MWNTs-NCO nanocomposites, while Z_c increased. For a given cooling rate, Z_c for MCPA6/MWNTs-NCO nanocomposites was higher than that for pure MCPA6 and $t_{1/2}$ for MCPA6/MWNTs-NCO nanocomposites was lower, signifying that the incorporation of MWNTs-NCO could accelerate the crystallization of MCPA6. Further, it can be seen that the Avrami equation could well fit to the non-isothermal crystallization data for pure MCPA6, however, in the late stage of crystallization, the equation deviate from the data for MCPA6/MWNTs-NCO nanocomposites, which is often attributed to secondary crystallization. It was meant that the non-isothermal crystallization of MCPA6/MWNTs-NCO nanocomposites is a more complicated process as compared with that of pure MCPA6.

Ozawa model

According to Ozawa theory [26], the non-isothermal crystallization process consist of an infinite number of small isothermal crystallization steps, and the degree of conversion as a function of temperature, X_T, can be expressed as

$$1 - X_T = \exp(-K(T)/\beta^m) \tag{8}$$

where $K(T)$ is the cooling crystallization function, m is Ozawa exponent that depends on the crystal growth and nucleation mechanism. The double logarithmic form of Eq. 8 is

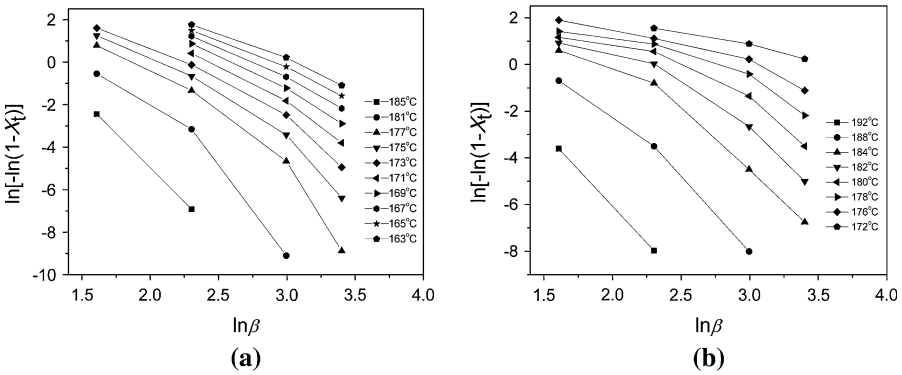

Fig. 5 Ozawa plots of $\ln[-\ln(1 - X_t)$ versus $\ln\beta$ for non-isothermal crystallization of **a** pure MCPA6 and **b** MCPA6/MWNTs-NCO nanocomposites

$$\ln[-\ln(1 - X_T)] = \ln K(T) - m \ln \beta \tag{9}$$

Figure 5 shows the Ozawa analysis results for polypropylene. A series of lines are obtained at different temperatures, and the line should be straight if the Ozawa method is valid. However, it can be seen obviously from the curves that the Ozawa plots of pure MCPA6 and MCPA6/MWNTs-NCO nanocomposites showed deviation from linearity, suggesting that the Ozawa equation could not describe the non-isothermal crystallization behaviors for both pure MCPA6 and MCPA6/MWNTs-NCO nanocomposites satisfactorily.

Mo model

Mo and his coworkers [27] developed a new method combining Avrami equation with the Ozawa equation to describe the non-isothermal crystallization kinetics of polymer. The modified equation is

$$\ln \beta = \ln F(T) - \alpha \ln t \tag{10}$$

where $F(T) = [K(T)/Z]^{1/m}$ refers to the cooling rate at unit crystallization time when the polymer reaches a certain value of relative crystallinity. α refers to the ratio of the Avrami exponent n to the Ozawa exponent $m(\alpha = n/m)$. Figure 6 presents the plots of $\ln\beta$ versus $\ln t$ at various degree crystallinities for pure MCPA6 and MCPA6/MWNTs-NCO nanocomposites. It can be seen that the plots show good linearity, verifying obviously that Mo method describe appropriately the non-isothermal crystallization kinetics of the system. The parameters $F(T)$and α are estimated from the intercept and slope of the lines, respectively, listed on Table 2. The value of α varies from 1.32 to 1.40 for pure MCPA6 and from 1.24 to 1.20 for the nanocomposites; while $F(T)$, mainly reflecting the crystallization facilitation effect of the nanoparticles on MCPA matrix, increases systematically with the increasing of the relative crystallinity, and is lower for the nanocomposites at the same relative crystallinity. It indicates that it has shorter time for MCPA6/MWNTs-NCO nanocomposites to achieve the same degree of crystallinity than for pure

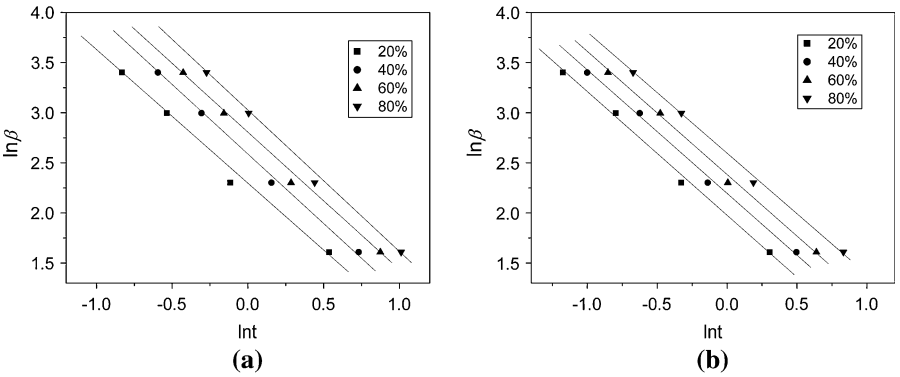

Fig. 6 Plots of $\ln\beta$ versus $\ln t$ for **a** pure MCPA6 and **b** MCPA6/MWNTs-NCO nanocomposites at different relative crystallinity

Table 2 Kinetic parameters for MCPA6 and MCPA6/MWNTs-NCO nanocomposites at different relative degrees of crystallinity based on Mo model

Sample	X_t (%)	α	$F(T)$
Pure MCPA6	20	1.32	9.58
	40	1.36	13.06
	60	1.38	15.96
	80	1.40	19.88
MCPA6/MWNTs-NCO	20	1.24	7.09
	40	1.22	8.93
	60	1.22	10.69
	80	1.20	13.19

MCPA6. The importance of Mo method is that it correlates the cooling rates to temperature, time and morphology [28].

Urbanovici–Segal model

Urabanovici and Segal [29] proposed a new kinetic equation, which is essentially a generalization of the Avrami model. In this model, the relationship between the time-dependent relative crystallinity function and the crystallization time t is given by

$$X(t) = 1 - [1 + (r_{US} - 1)(K_{US}t)^{n_{US}}]^{1/(1-r_{US})} \quad (11)$$

where K_{US} and n_{US} are the Urbanovici–Segal crystallization rate constant and the Urbanovici–Segal exponent, respectively, and r_{US} denotes the deviation degree between Urbanovici–Segal model and Avrami model. As $r_{US} \rightarrow 1$, the Urbanovici–Segal equation becomes identical to Avrami equation [29], and it is worth noting that the Urbanovici–Segal kinetics parameters, K_{US} and n_{US}, have a similar physical meaning to the Avrami kinetics parameters, Z and n, respectively. Zhou [30] also

Table 3 Kinetic parameters for MCPA6 and MCPA6/MWNTs-NCO nanocomposites at different relative degrees of crystallinity based on Urbanovici–Segal model

Sample	β (°C min^{-1})	K_{US}	n_{US}	r_{US}	r^2
Pure MCPA6	5	0.40	4.00	0.97	0.9998
	10	0.75	3.45	0.95	0.9996
	20	1.10	3.36	0.88	0.9995
	30	1.45	3.02	0.85	0.9992
MCPA6/MWNTs-NCO	5	0.55	4.62	1.71	0.9997
	10	1.02	4.34	1.52	0.9996
	20	1.68	5.01	1.61	0.9994
	30	1.67	4.94	1.57	0.9989

employed this model to describe the non-isothermal crystallization process of isotactic polypropylene and its blend with ethylene–octane.

The parameters of this model for the non-isothermal crystallization of pure MCPA6 and MCPA6/MWNTs-NCO nanocomposites were listed in Table 3, and the curves of the model fitted to the experimental data for both samples are presented in Fig. 7. The values of correction coefficient (r^2) are all close to 1, verifying that this model could well description of the non-isothermal crystallization process of the system. It is obvious that the values of r_{US} for pure MCPA6 are closer to 1 than that for its nanocomposites, indicating that the non-isothermal crystallization kinetics of its nanocomposites deviate more from the Avrami model, which is consistent with the result analyzed via Avrami method.

Effective activation energy for non-isothermal crystal growth

For non-isothermal crystallization process, it is also interesting to obtain effective activation energy E, and Kissinger method [31] was one of the most popular approaches for calculating the effective activation energy of non-isothermal crystallization. However, Vyazovkin [32] demonstrated that Kissinger equation appears to be inapplicable for evaluating the activation energy of the processes that occurred on cooling, and verified that using the isoconversional methods developed by Friedman [33] or by Vyazovkin and coworkers [34, 35] can obtained the correct values. In this investigation, Friedman method was used and its equation can be expressed as:

$$\ln\left(\frac{\mathrm{d}X}{\mathrm{d}t}\right)_{X,i} = \text{constant} - \frac{E_X}{RT_{X,i}} \tag{12}$$

where $(\mathrm{d}X/\mathrm{d}t)_{X,i}$ is the instantaneous crystallization rate at a given relative crystallinity, X, and i is the ordinal number of the experiment carried out at the cooling rate, β_i. E_X is the effective energy barrier of the process at the given value of X. By plotting the left hand side of Eq. 12 with respect to $1/T_X$ at different cooling rates, a straight line must be obtained with a slope equal to $-E_X/R$. Some works

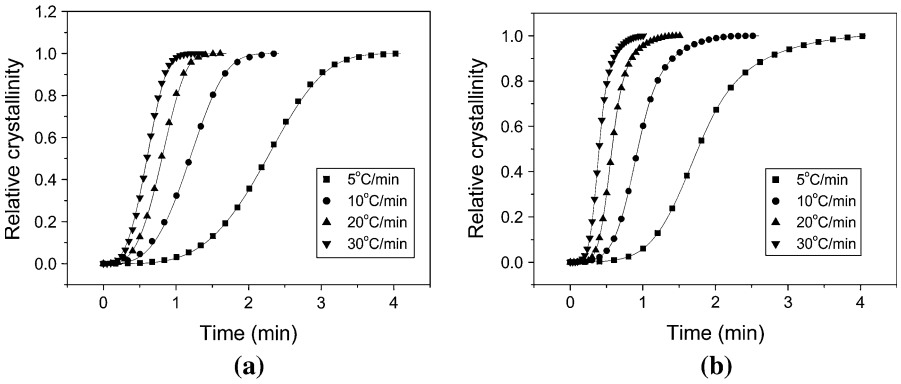

Fig. 7 The comparison between the results via Urbanovici–Segal model and experimental data: **a** pure MCPA6 and **b** MCPA6/MWNTs-NCO nanocomposites. *Solid lines* are the results via Urbanovici–Segal model

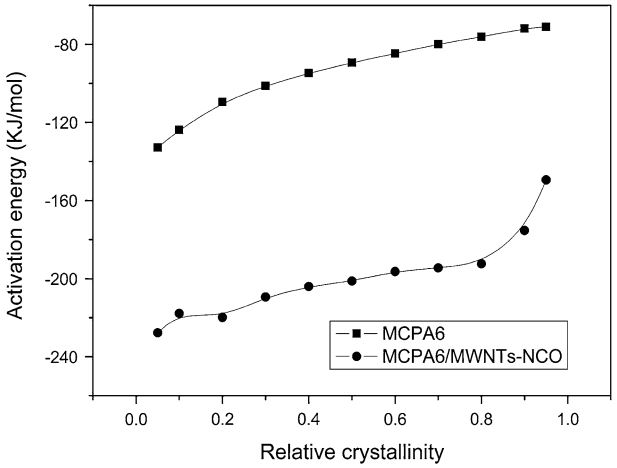

Fig. 8 Dependence of the effective activation energy on the extent of relative crystallinity

[28, 36] have used this method to calculate the effective activation energy for polymer crystallization.

The dependence of the effective activation energy on the relative crystallization for pure MCPA6 and its nanocomposites is presented in Fig. 8. As it can be seen that for both samples, E increases with the increase in the relative degree of crystallinity, which indicates non-isothermal crystallization becomes more difficult with increasing X. The apparent activation energy includes nucleating effect and retarding effect. The value of E for MCPA6/MWNTs-NCO nanocomposites greatly lower than that for pure MCPA6, which could be explained by that there is a strong interaction between the functionalized carbon nanotubes and MCPA6, therefore, the molecular chains crystallize more readily in MCPA6/MWNTs-NCO nanocomposites than in pure MCPA6. The results suggests that the addition of 0.3 wt%

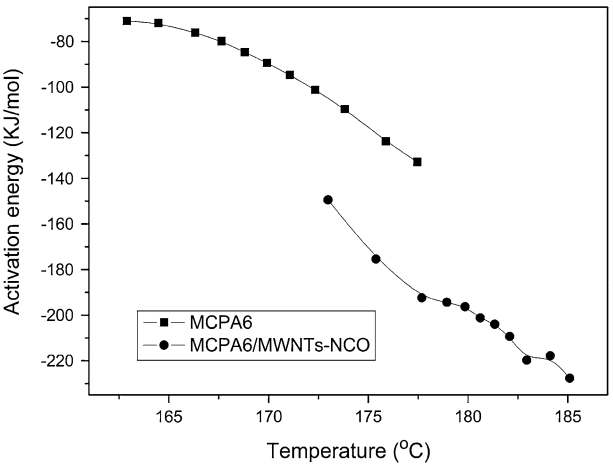

Fig. 9 The relation of effective activation energy versus average temperature

MWNTs-NCO cause nucleating effect dominating over retarding effect in the crystallization process. Accordingly, the addition of MWNTs-NCO could accelerate the overall non-isothermal process of MCPA6.

Furthermore, according to Vyazovkin [37], the effective activation energy can be plotted as a function of temperature by taking an average temperature corresponding to certain relative crystallinity X (Fig. 9); and these plots can be used to evaluate the Lauritzen–Hoffman parameters.

Conclusions

MCPA6/MWNTs-NCO nanocomposites were prepared via anionic polymerization of CL, and the functionalized MWNTs present good interfacial adhesion with MCPA6 matrix. In non-isothermal crystallization kinetics, the Avrami plots showed good linearity for pure MCPA6, however, the data for MCPA6/MWNTs-NCO nanocomposites in later stage of crystallization deviate from linearity; the Ozawa analysis failed to provide adequate description of the non-isothermal crystallization of both samples; the Mo and Urbanovici–Segal models can describe well the non-isothermal crystallization kinetics of the system. The effective activation energy for non-isothermal crystallization was evaluated by using Friedman equation. It was found that the energy varied with the degree of crystallinity and the addition of MWNTs-NCO could remarkably decrease the effective activation energy.

Acknowledgments We gratefully acknowledge the Important Item of Science and Technology of Fujian province (Grand No. 2007HZ0001-2) for the financial support. We are also grateful to the Center Laboratory of Fuzhou University for provision of testing facilities.

References

1. Crespy D, Landfester K (2005) Anionic polymerization of ε-caprolactam in miniemulsion: synthesis and characterization of polyamide-6 nanoparticles. Macromolecules 38:6882–6887
2. Liu A, Xie T, Yang G (2006) Synthesis of exfoliated monomer casting polyamide 6/Na^+-montmorillonite nanocomposites by anionic ring opening polymerization. Macromol Chem Phys 207: 701–707
3. Rusu G, Ueda K, Rusu E et al (2001) Polyamides from lactams by centrifugal molding via anionic ring-opening polymerization. Polymer 42:5669–5678
4. Leblanc JL (2002) Rubber–filler interactions and rheological properties in filled compounds. Prog Polym Sci 27:627
5. Wu D, Zhou C, Hong Z et al (2005) Study on rheological behaviour of poly(butylene terephthalate)/montmorillonite nanocomposites. Eur Polym J 41:2199–2207
6. Ray SS, Okamoto M (2003) Polymer/layered silicate nanocomposites: a review from preparation to processing. Prog Polym Sci 28:1539–1641
7. Spitalsky Z, Tasis D, Papagelis K et al (2010) Carbon nanotube–polymer composites: chemistry, processing, mechanical and electrical properties. Prog Polym Sci 35:357–401
8. Wu TM, Chang HL, Lin YW (2009) Synthesis and characterization of conductive polypyrrole/multiwalled carbon nanotubes composites with improved solubility and conductivity. Compos Sci Technol 69:639–644
9. Al-Rawajfeh AE, Al-Salah HA, AlShamaileh E et al (2008) Polyamide-based composite membranes: part 2. Interaction, crystallization and morphology. Desalination 227:120–131
10. Custodio F, Steenbakkers RJA, Anderson PD et al (2009) Model development and validation of crystallization behavior in injection molding prototype flows. Macromol Theory Simul 18:469–494
11. Kim KH, Isayev AI, Kwon K (2005) Flow-induced crystallization in the injection molding of polymers: a thermodynamic approach. J Appl Polym Sci 95:502–523
12. Zhao C, Zhang P, Yi L et al (2008) Study on the non-isothermal crystallization kinetics of novel polyamide 6/silica nanocomposites containing epoxy resins. Polym Test 27:412–419
13. Yuan Q, Awate S, Misra RDK (2006) Nonisothermal crystallization behavior of polypropylene–clay nanocomposites. Eur Polym J 42:1994–2003
14. Hao W, Yang W, Cai H et al (2010) Non-isothermal crystallization kinetics of polypropylene/silicon nitride nanocomposites. Polym Test 29:527–533
15. Xu JT, Wang Q, Fan ZQ (2005) Non-isothermal crystallization kinetics of exfoliated and intercalated polyethylene/montmorillonite nanocomposites prepared by in situ polymerization. Eur Polym J 41:3011–3017
16. Kim HJ, Lee JJ, Kim JC et al (2010) Effect of starch content on the non-isothermal crystallization behavior of HDPE/silicate nanocomposites. J Ind Eng Chem 16:406–410
17. Weng W, Chen G, Wu D (2003) Crystallization kinetics and melting behaviors of nylon 6/foliated graphite nanocomposites. Polymer 44:8119–8132
18. Guo B, Zou Q, Lei Y et al (2009) Crystallization behavior of polyamide 6/halloysite nanotubes nanocomposites. Thermochim Acta 484:48–56
19. Liu Y, Yang G (2010) Non-isothermal crystallization kinetics of polyamide-6/graphite oxide nanocomposites. Thermochim Acta 500:13–20
20. Kuo MC, Huang JC, Chen M (2006) Non-isothermal crystallization kinetic behavior of alumina nanoparticle filled poly(ether ether ketone). Mater Chem Phys 99:258–268
21. Li J, Fang Z, Tong L et al (2006) Effect of multi-walled carbon nanotubes on non-isothermal crystallization kinetics of polyamide 6. Eur Polym J 42:3230–3235
22. Lorenzo MLD, Cimmino S, Silvestre C (2001) Nonisothermal crystallization of isotactic polypropylene blended with poly(a-pinene). I. Bulk crystallization. J Appl Polym Sci 82:358–367
23. Wunderlich B (1997) Thermal characterization of polymeric materials. In: Turi E (ed) 2rd. Academic Press, New York, pp 205–482
24. Avrami M (1939) Kinetics of phase change. J Chem Phys 7:1103
25. Jeziorny A (1978) Parameters characterizing the kinetics of the non-isothermal crystallization of poly(ethylene terephthalate) determined by d.s.c. Polymer 19:1142–1144
26. Ozawa T (1971) Kinetics of non-isothermal crystallization. Polymer 12:150–158
27. Liu TX, Mo ZS, Wang SE (1997) Nonisothermal melt and cold crystallization kinetics of poly(arylether ether ketone ketone). Polym Eng Sci 37:568–575

28. Papageorgiou GZ, Achilias DS, Bikiaris DN et al (2005) Crystallization kinetics and nucleation activity of filler in polypropylene/surface-treated SiO_2 nanocomposites. Thermochim Acta 427: 117–128
29. Urbanovici E, Segal E (1990) New formal relationships to describe the kinetics of crystallization. Thermochim Acta 171:87–94
30. Zhou H, Ying J, Xie X et al (2010) Nonisothermal crystallization behavior and kinetics of isotactic polypropylene/ethylene–octene blends. Part II: modeling of crystallization kinetics. Polym Test 29:915–923
31. Kissinger HE (1956) Variation of peak temperature with heating rate in differential thermal analysis. J Res Natl Stand 57:217–221
32. Vyazovkin S (2002) Is the Kissinger equation applicable to the processes that occur on cooling? Macromol Rapid Commun 23:771–775
33. Friedman HL (1964) Kinetics of thermal degradation of char-forming plastics from thermogravimetry. J Polym Sci C 6:183
34. Vyazovkin S (2001) Modification of the integral isoconversional method to account for variation in the activation energy. J Comput Chem 22:178–183
35. Vyazovkin S (1997) Evaluation of activation energy of thermally stimulated solid-state reactions under arbitrary variation of temperature. J Comput Chem 18:393–402
36. Qiu S, Zheng Y, Zeng A et al (2011) Prediction of non-isothermal crystallization parameters for isotactic polypropylene. Thermochim Acta 512:28–33
37. Vyazovkin S, Sbirrazzuoli N (2004) Isoconversional approach to evaluating the Hoffman–Lauritzen parameters (U* and Kg) from the overall rates of nonisothermal crystallization. Macromol Rapid Commun 25:733–738